2022 IEEE International Conference on Robotics and Automation (ICRA)
May 23-27, 2022. Philadelphia, PA, USA

Forward Models That Integrate High-Dimensional and Localized Sensing of Peripheral Muscle Behavior Enable Task-Independent Prediction of Lower-Limb Joint Torque and Position Future States

Kaitlin G. Rabe, *Student Member, IEEE* and Nicholas P. Fey, *Member, IEEE*

***Abstract*— We develop a task-independent predictive framework that estimates hip, knee and ankle future behavior from sonomyographic sensing of quadriceps musculature. Two regression models, support vector regression and Gaussian process regression, were trained and tested such that no ambulation mode recognition was required. Sonomyography features of the anterior thigh musculature were extracted during the swing phase of level, incline and stair ambulation tasks as inputs to the two models for continuous prediction of the future stance phase hip, knee and ankle moments. Next, sonomyography features of the anterior thigh musculature were extracted during the stance phase and used to predict the following swing phase hip, knee and ankle angles. Leave-one-stride-out cross-validation is used to evaluate this continuous prediction framework. Additionally, initial, peak and terminal joint moment and angle parameters are extracted from trajectories and evaluated. Both regression models were able to accurately predict continuous future joint moments and angles, as well as initial, peak and terminal value parameters of future joint moments and angles. However, the support vector regression model required relatively lower computational cost. Thus, we recommend the support vector regression model as an optimal model for forward prediction of joint mechanics from sonomyographic sensing during ambulation.**

***Index Terms*—Machine Learning for Robot Control, Prosthetics and Exoskeletons, Sensor-Based Control**

I. Introduction

Wearable robotic assistive devices can generate net mechanical power to assist or restore mobility to their users [1]. One device objective is to restore a disabled limb's motor function to normal levels [2]. Currently-available technologies are commonly used to provide basic functionality, such as standing or level-ground walking. Wearable robots can enable greater functionality to their users by returning biologically-accurate torque at to their joints [3]. However, to achieve robust control, hierarchical control structures are commonly implemented wherein at the highest level an activity mode is classified, and subsequently device parameters are adjusted based on various reference trajectories within each activity mode, as well as specific phases of each mode [4]–[6]. Alternatively, volitional and semi-volitional control approaches could provide users a greater level of command over their device during continuously-varying activities. However, volitional control requires a continuous joint-level input to direct future continuous joint-level responses—For example estimating future joint angles or moments without the requirement of a pre-defined locomotor task label. Semi-volitional control can be implemented in a variety of ways: one possibility is to predict specific parameters related to the desired motion that dictate the device output (e.g., quasi-stiffness, peak joint angle, and terminal joint angle [7], [8]).

To optimize control schemes during weight-bearing tasks, such as stance phase of gait, continuous prediction of joint moments or torques (for volitional control), or parameters related to joint moment (for semi-volitional control) are beneficial to effectively manage the interaction of the foot with the ground and provide optimal energy to the user [9]. During non-weight-bearing tasks, position-based controllers have been proposed as an optimal control strategy to ensure flexibility within the device to change position when not interacting with the ground [10], [11]. Both volitional and semi-volitional control rely on accurate sensing and precise mapping to device parameters. Sonomyography, or the evaluation of real-time ultrasound imaging of skeletal muscle, has been proposed as a high dimensional and localized sensing modality for robust control over multiple degree-of-freedom robotic prosthetic hands [12]–[14], torque control of an ankle exoskeleton [15], [16], and accurate estimation of ambulation mode [17], as well as continuous estimation of knee angle [18] and hip, knee and ankle moments [19]. However, sonomyography has not been evaluated for *future prediction* of continuous trajectories or parameterized features of hip, knee and ankle joint kinematics or kinetics during varying ambulation tasks.

We explore two commonly used supervised machine learning approaches in this study. Support vector regression (SVR) is a robust non-parametric approach for classification and function regression [20]. SVR is effective in high dimensional spaces (e.g., high dimensional sonomyography data) and use only a subset of training points in the decision function, improving memory efficiency and computational demand. However, SVR performance can decrease with noisy datasets. Previous researchers have utilized SVR for generating trajectories for walking humanoid robots, as well as to improve myoelectric simultaneous control of multiple degrees-of-freedom [21], [22]. Gaussian process regression (GPR) is a non-parametric Bayesian approach for solving non-linear regression [23], and has demonstrated success for modeling nonlinear dynamical systems such as human motion [24]. GPR produces probabilistic predictions that account for

This work was supported by the National Science Foundation (grant 1925343).

K. G. Rabe is with the Department of Biomedical Engineering at The University of Texas at Austin, Austin, TX 78712 USA. (email: kaitlin.rabe@utexas.edu).

N. P. Fey is with the Walker Department of Mechanical Engineering at The University of Texas at Austin, Austin, TX 78701 USA. (email: nfey@utexas.edu).

2022 IEEE International Conference on Robotics and Automation (ICRA) | 978-1-7281-9681-7/22/$31.00 ©2022 IEEE | DOI: 10.1109/ICRA46639.2022.9812035

inherent noise within the input feature set. However, GPR requires storage of the entire feature set for prediction, which can increase computational demand. The objective of both models is to fine tune precision, cost and the kernel regulator to optimize the trade-off between model complexity and output accuracy. We optimize these models for prediction of future continuous hip, knee and ankle joint moments during stance and joint angles during swing from sonomyography. Additionally, initial, peak and terminal values of the hip, knee and ankle moments and angles are predicted during stance and swing, respectively.

The overall objective of this work is to develop and test a computational framework for sonomyography as an input to GPR and SVR models for both continuous prediction of future joint moments and angles, as well as parameters of future joint moments and angles. *We hypothesize that sonomyography will enable accurate prediction of continuous joint trajectories via GPR and SVR, but that GPR will result in greater accuracy (lower error) for its ability to handle noisy datasets in comparison to SVR. Furthermore, we hypothesize that the GPR model prediction of joint moment and angle trajectories will result in greater accuracy of target parameters (namely, initial, peak and terminal values) in comparison to the SVR model prediction.* In future studies, the ability to infer future joint moment and angle trajectories and parameters allows time for pre-processing and feature extraction, as well as for mapping of control inputs to device actuation. Furthermore, it would be beneficial if the input to these different control outputs (joint angles and moments) can be commanded by the same localized peripheral sensing modality (e.g., sonomyography).

II. Methods

A. Data Collection

Ten able-bodied subjects (five males, five females) gave informed consent prior to participating in this experiment. The experimental protocol was approved by the institutional review board. Subjects were asked to complete five ambulation tasks at a self-selected speed: (1) level walking, (2) 10° incline walking, (3) 10° decline walking, (4) stair ascent and (5) stair descent. Walking trials were completed on a split-belt force-instrumented treadmill (Bertec Corporation) for one-minute. Stair trials were completed on a four-step staircase, beginning with stair ascent and followed by stair descent for five repetitions with a step-over-step alternating pattern.

During the locomotion experiment, subjects were equipped with a 128-element linear array ultrasound transducer affixed to the anterior thigh of their non-dominant limb via a custom-designed holder. The transducer of a handheld and wearable ultrasound system (mSonics, Lonshine Technologies Inc.) was placed transversely on the anterior thigh to collect real-time cross-sectional images of the rectus femoris, vastus medialis and vastus intermedius muscles with a transmit frequency of 7.5 MHz. Prior to the beginning of the locomotion experiment, US beam depth was adjusted to ensure a clear image from the superficial transducer-skin interface to the deep vastus intermedius boundary, balancing the effects of spatial resolution with penetration depth.

Reflective markers were placed over anatomical landmarks for collection of joint kinematic and kinetic data using a ten-camera motion capture system (VICON Motion Systems, Inc.) with a sampling rate of 1000 Hz. Ground reaction force data were recorded from force plates within the instrumented treadmill with a sampling rate of 100 Hz. All data were recorded to the same computer with time-stamping for synchronization of ultrasound, kinematic and kinetic data.

B. Signal Processing

Ultrasound imaging is commonly used to visualize underlying soft tissue in the body, including skeletal muscle during movement [25]. Changes in muscle architecture, such as muscle thickness and cross-sectional area, as well as spatial changes in intensity of the grayscale ultrasound images have previously been correlated with changes in muscle strength [26], the onset of muscle contraction [27], [28], muscle force production [29] and resulting joint motion [14], [18]. Therefore, we extracted image intensity, as well as time-derivative intensity sonomyography features from each frame of ultrasound for prediction of hip, knee and ankle joint mechanics. A spatial filter with a 3x3 mm block size was used reduce motion artifact and the mean intensity of each block was calculated. This resulted in 260 total 3x3 mm blocks of mean intensity. The 2-dimensional image array was reshaped into 1-dimension by horizontally concatenating each row of ultrasound features ranging from superficial to deep tissue. Next, the time derivative was taken between each consecutive frame of 260 ultrasound features, growing the feature set to 520 total features of sonomyography for each ultrasound frame.

Hip, knee and ankle moments and angles were calculated using Visual 3D (C-Motion, Inc.) via inverse kinematics and dynamics. Resulting joint moments and angles were low-pass filtered to reduce signal noise. Due to the lack of force plates in the stairs, ground reaction force data was not captured during stair ascent or stair descent and no joint moment data could be calculated for these ambulation tasks. Joint angle data were available for all five ambulation tasks. Heel strike and toe off events were recorded for all ambulation tasks. All sonomyography features, joint moment and angle datasets were segmented by heel strikes of the ultrasound-equipped limb. Next, sonomyography features were z-normalized for each subject, then split into separate datasets for stance and swing phases of each ambulation task. Hip, knee and ankle moments and angles were also split into stance and swing phases, respectively. Finally, all stance and swing sonomyography features, stance joint moment and swing joint angle vectors were resampled to 20 Hz to ensure the all vectors were the same length for regression implementation.

C. Regression Models

Two regression models, SVR and GPR, were evaluated for continuous estimation of hip, knee and ankle moments during stance, and hip, knee and ankle angles during swing. For a detailed explanation of the SVR and GPR models please refer to [20] and [23], respectively. For both models, the kernel was

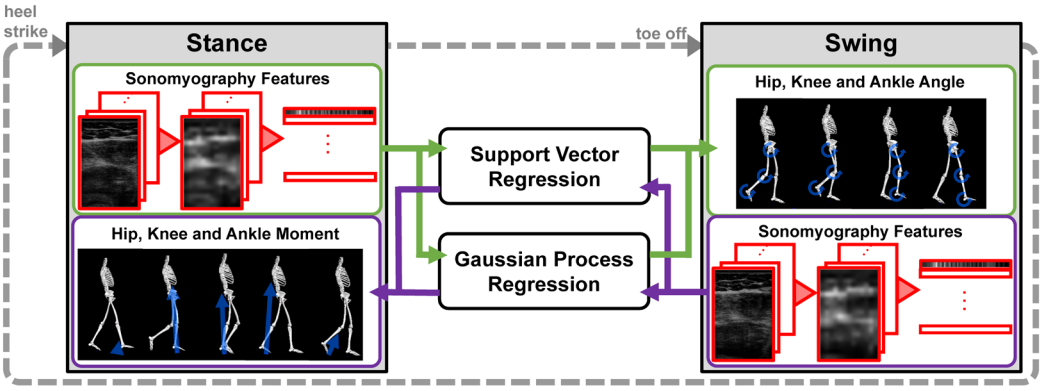

Figure 1. Predictive Control Framework for Swing Phase Joint Angles and Stance Phase Joint Moments. S*onomyography features were extracted during stance and fed to support vector regression (SVR) and Gaussian process regression (GPR) models for continuous prediction of future hip, knee and ankle angle during swing (top). Sonomyography features were extracted from ultrasound images acquired during swing and fed to SVR and GPR models for continuous prediction of the following gait cycle's hip, knee and ankle moment during stance (bottom).*

optimized to balance overfitting and model complexity. The radial basis function kernel was used for SVR, which computes the similarity of two points, X_1 and X_2, and is described by:

$$K(X_1, X_2) = \exp(-\frac{\|X_1 - X_2\|^2}{2\sigma^2}), \quad (1)$$

where σ is the variance, and $\|X_1 - X_2\|$ is the Euclidean distance between two points X_1 and X_2. This kernel is beneficial for reducing the complexity of the SVR learning problem by reducing the amount of training data stored by the model [30]. The rational quadratic kernel was used for GPR, which can be described as an infinite sum of radial basis function kernels with different characteristic length scales, l. The rational quadratic kernel is defined as:

$$K(X_1, X_2) = \left(1 + \frac{\|X_1 - X_2\|^2}{2\alpha l^2}\right)^{-\alpha}, \quad (2)$$

where α is the scale-mixture parameter and must be greater than zero [23]. This kernel is beneficial for predicting functions that vary smoothly across many length-scales which is advantageous for large datasets [31].

Sonomyography features from stance were used to train the SVR and GPR models for continuous prediction of the following swing phase hip, knee and ankle angles; and sonomyography features from swing were used to train the SVR and GPR models for continuous prediction of the subsequent stance phase hip, knee and ankle moment (Fig. 1). Both the SVR and GPR models were trained on task-independent datasets containing sonomyography features from strides of all ambulation tasks. Twenty strides of each level, incline and decline walking tasks were included in all models; and, the maximum number of stair ascent and descent strides available (up to twenty) were added to the models for joint angle prediction during swing only (due to missing ground reaction force data from stair ambulation tasks). Transition strides (walk-to-stair/stair-to-walk) were included in the stair ascent and stair descent datasets to maximize the number of strides available. Leave-one-stride-out cross-validation was used to minimize over-fitting of the models where one stride of each ambulation tasks' stance and swing data was removed from the training dataset for testing, looping through all strides such that each stride was the test stride once. To compare parameters for semi-volitional control structures, initial, peak and terminal joint moments and angles were extracted from the model's prediction of future stance and swing, and compared to the measured initial, peak and terminal moments and angles.

D. Model Evaluation and Statistical Methods

Root mean square errors (RMSE) were calculated between the SVR and GPR model's predictions of joint moments and angles and the measured joint moments and angles. Paired t-tests were used to compare RMSE from SVR and GPR for each joint and ambulation mode (α=0.05). An additional goodness of fit metric, adjusted coefficient of determination (R^2) for nonlinear regression, was calculated for each of the SVR and GPR predictions of joint moments and angles in comparison to the measured joint moments and angles.

Initial, peak and terminal joint moment and angle parameters were extracted from the SVR and GPR prediction of stance and swing. Means and standard deviation (SD) absolute differences between parameters from SVR and GPR models with the measured initial, peak and terminal joint moments and angles were calculated. Paired t-tests were used to evaluate a significance between the SVR and GPR parameter differences (α=0.05). A significance level of p<0.05 was set for all tests.

III. Results

Ten able-bodied subjects participated in the locomotion experiment for training and testing the predictive framework (TABLE I). As hypothesized, both the SVR and GPR models resulted in high accuracy of both continuous future prediction of hip, knee and ankle moment during stance, as well as hip, knee, and ankle angle during swing. Additionally, both models resulted in high accuracy of initial, peak and terminal parameters of hip, knee and ankle moment during stance, as well as hip, knee and ankle angle during swing. However, there were inconsistencies between which model performed better at varying joint levels and ambulation tasks.

A. Continuous Prediction of Future Hip, Knee and Ankle Mechanics

Both the SVR and GPR models were able to predict the general trends and variability of hip, knee and ankle moment

TABLE I. MEAN AND STANDARD DEVIATION (SD) PARTICIPANT CHARACTERISTICS.

Participant Characteristic	Mean (SD)
Age (years)	29.5 (10.6)
Level Walk Speed (m/s)	0.8 (0.1)
Incline Walk Speed (m/s)	0.6 (0.1)
Decline Walk Speed (m/s)	0.6 (0.1)
Number of Stair Ascent Strides (#)	9.4 (3.5)
Number of Stair Descent Strides (#)	9.3 (5.7)

during stance from sonomyography features extracted from the previous gait cycle's swing phase (Fig. 2). Overall, averaging across all ambulation modes at each joint, the GPR model resulted in reduced RMSE of joint moment prediction in comparison to the SVR model, however there were no significant differences between the overall joint moment RMSEs during stance (TABLE II). The GPR model resulted in significantly improved prediction (lower RMSE) compared to the SVR models' prediction of knee and ankle moment during level walking and knee moment during decline walking.

Similarly, the SVR and GPR models trained using sonomyography features extracted during stance were able to accurately predict the mean and variability of future swing hip, knee and ankle joint angles during level, incline, decline, stair ascent and stair descent ambulation (Fig. 2). However, the SVR model resulted in reduced (or equal) RMSE of future swing joint angle prediction averaged across all ambulation tasks at each joint, although there were no significant differences between the SVR and GPR models. The only significant differences between RMSE of the SVR and GPR prediction of joint angle were observed when comparing knee angle during level walk and ankle angle during stair ascent. In both cases, the SVR model significantly improved the angle prediction (TABLE II).

B. Prediction of Future Hip, Knee and Ankle Parameters

Initial, peak and terminal values of joint moment during stance and joint angle during swing were extracted from the continuous predictive models as possible parameters for a semi-volitional control framework. Absolute differences between parameters extracted from SVR and GPR models with the measured parameters during stance and swing were calculated (TABLE III). Based on the absolute differences of joint parameters, the highest error of joint moment parameter estimation was observed during decline walking, while the highest error of joint angle parameter estimation occurred during stair descent.

Comparing initial joint moment parameters, the GPR model resulted in a significant reduction in absolute difference between the model's prediction and estimated joint moment parameter at the hip during level walking, knee during incline walking, and ankle during level and decline walking tasks. Comparing differences in peak moment prediction, there were significant differences between the SVR and GPR prediction of hip moment during incline and decline walking, knee during level walking, and ankle during incline and decline walking. Additionally, comparing terminal joint moment parameters, significant differences were observed at the hip during all walking tasks, and at the knee and ankle during level walking. There were inconsistencies comparing which model (SVR or GPR) resulted in the significantly reduced error between predicted peak and terminal joint moments and measured peak and terminal joint moments.

Both the SVR and GPR resulted in accurate future prediction of initial, peak and terminal joint angles during swing of all walking tasks. Comparing initial joint angles, the only significant difference was observed at the knee during level walking where the GPR model reduced error between predicted measured initial knee angle. Comparing peak angles, the SVR model consistently resulted in significantly

TABLE II. ROOT MEAN SQUARE ERROR (RMSE) AND ADJUSTED R^2 COMPARING SUPPORT VECTOR REGRESSION AND GAUSSIAN PROCESS REGRESSION ESTIMATES OF HIP, KNEE AND ANKLE MOMENT (TOP) AND HIP, KNEE AND ANKLE ANGLE (BOTTOM).

Stance Prediction	Mean (SD) RMSE Moment (Nm/kg)			Adjusted R^2		
	Hip	Knee	Ankle	Hip	Knee	Ankle
Support Vector Regression (SVR)						
Level Walk	0.16 (0.05)	0.09 (0.04)[a]	0.14 (0.07)[a]	0.86	0.84	0.88
Incline Walk	0.16 (0.09)	0.18 (0.08)	0.27 (0.14)	0.94	0.88	0.83
Decline Walk	0.33 (0.19)	0.26 (0.13)[a]	0.12 (0.06)	0.88	0.83	0.92
Overall	**0.21 (0.14)**	**0.18 (0.12)**	**0.17 (0.11)**	**0.89**	**0.85**	**0.88**
Gaussian Process Regression (GPR)						
Level Walk	0.12 (0.05)	0.08 (0.04)[a]	0.09 (0.03)[a]	0.92	0.85	0.95
Incline Walk	0.20 (0.12)	0.19 (0.10)	0.21 (0.12)	0.88	0.86	0.90
Decline Walk	0.30 (0.18)	0.23 (0.18)[a]	0.11 (0.06)	0.90	0.87	0.93
Overall	**0.20 (0.14)**	**0.17 (0.11)**	**0.14 (0.10)**	**0.90**	**0.95**	**0.93**

Swing Prediction	Mean (SD) RMSE Angle (deg)			Adjusted R^2		
	Hip	Knee	Ankle	Hip	Knee	Ankle
Support Vector Regression (SVR)						
Level Walk	1.24 (0.41)	2.33 (0.79)[a]	0.82 (0.26)	0.98	0.99	0.96
Incline Walk	1.91 (0.71)	3.03 (3.04)	1.53 (1.66)	0.98	0.96	0.95
Decline Walk	1.26 (0.74)	3.30 (1.00)	0.61 (0.19)	0.92	0.98	0.95
Stair Ascent	3.57 (1.28)	6.06 (1.82)	2.75 (0.74)[a]	0.96	0.94	0.95
Stair Descent	2.78 (0.97)	11.32 (4.33)	5.06 (1.94)	0.67	0.88	0.83
Overall	**2.15 (1.24)**	**5.20 (4.15)**	**2.15 (2.01)**	**0.90**	**0.95**	**0.93**
Gaussian Process Regression (GPR)						
Level Walk	1.11 (0.32)	2.53 (0.77)[a]	0.84 (0.27)	0.98	0.99	0.96
Incline Walk	1.95 (0.73)	3.37 (4.04)	1.41 (1.24)	0.98	0.94	0.95
Decline Walk	1.17 (0.66)	3.58 (1.30)	0.62 (0.31)	0.93	0.98	0.93
Stair Ascent	3.71 (1.32)	7.13 (1.97)	2.86 (1.09)[a]	0.85	0.91	0.93
Stair Descent	2.81 (0.92)	11.87 (4.46)	5.13 (2.15)	0.68	0.86	0.82
Overall	**2.15 (1.30)**	**5.70 (4.48)**	**2.17 (2.06)**	**0.91**	**0.94**	**0.92**

a. Significant difference ($p<0.05$) between RMSE of SVR and GPR prediction of joint trajectory

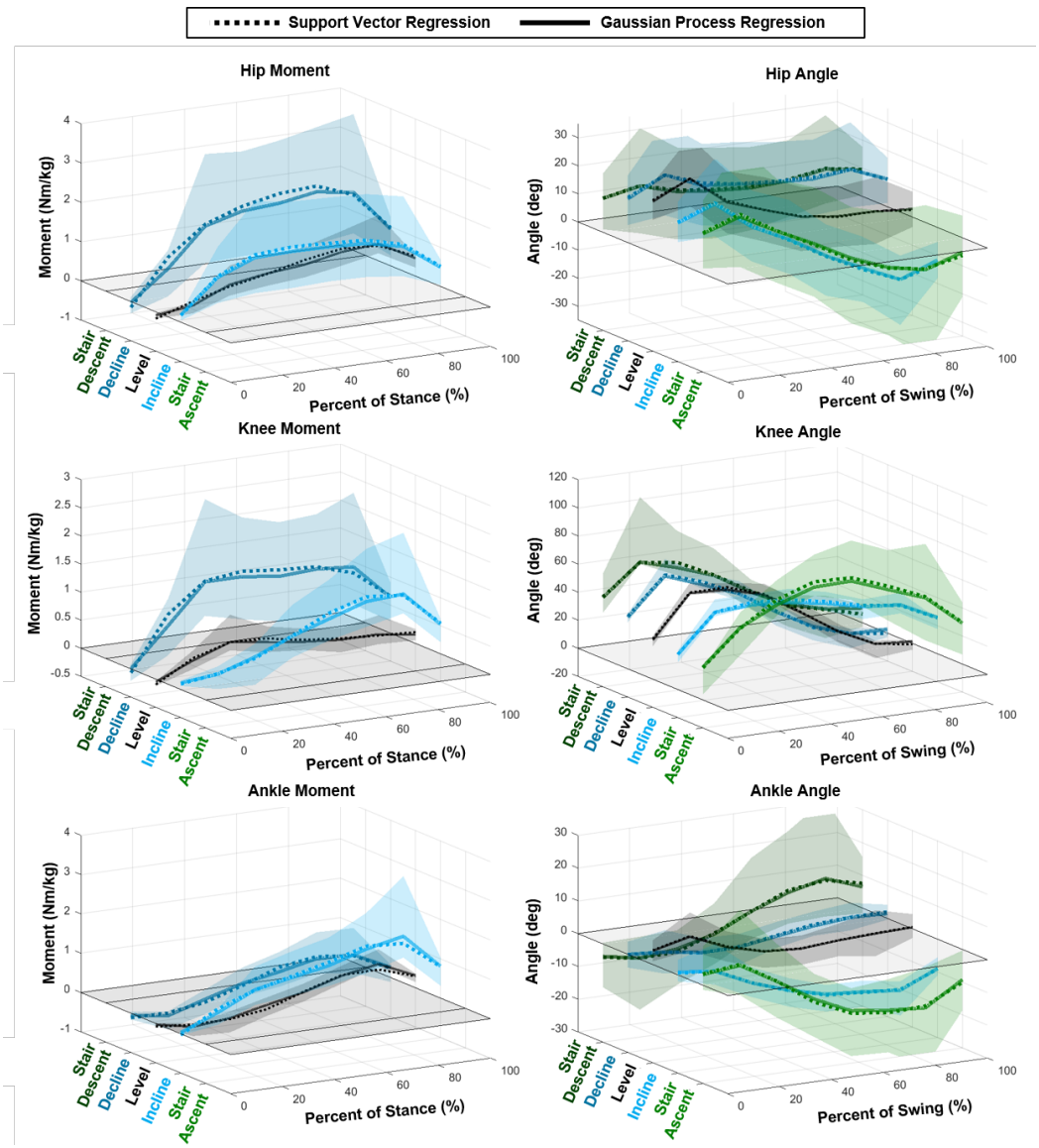

Figure 3. Hip, Knee and Ankle Moments During Stance and Hip, Knee and Ankle Angles During Swing of Five Ambulation Tasks. *Stance phase joint moments were predicted from SVR and GPR models trained on sonomyography features collected during the previous stride's swing phase. Swing phase joint angles were predicted from SVR models trained on sonomyography features collected during stance. Box plots display median, interquartile ranges and outliers. Standard deviations of measured joint moments and angles displayed in shaded regions for each ambulation mode. SVR and GPR mean (N=10) predictions joint moments and joint angles of shown as solid (GPR) and dashed lines (SVR).*

reduced error between predicted and measured angle at the hip joint during stair ascent, and at the knee and ankle joints during decline walking and stair ascent. Lastly, comparing terminal angle differences between predictive model and measured angle, the GPR model significantly reduced hip angle error during incline walking while the SVR model significantly reduced knee angle error during level walking and stair descent.

C. Computational Time

All signal processing, extraction of sonomyography features and implementation of the SVR and GPR models were completed offline on a single CPU (Intel(R) Core i7-7700 at 3.60 GHz). Mean (SD) time to extract features from a single frame of ultrasound was 19.4 (4.9) msec. Mean (SD) time to train and test the SVR models for stance prediction were 103.2 (8.2) and 1.6 (0.4) msec, respectively. Mean (SD) time to train and test the GPR models for stance prediction were and 843.9 (72.8) and 2.0 (0.8) msec, respectively. Mean (SD) time to train and test the SVR models for swing prediction were 98.0 (6.3) and 1.7 (0.5) msec, respectively. Mean (SD) time to train and test the GPR models for swing prediction were 1906.7 (161.1) and 3.6 (1.5) msec, respectively.

IV. Discussion

We developed a task-independent predictive framework for control of powered hip, knee and ankle joints using sonomyography features of the anterior thigh and two forward regression models. Surprisingly, there were few significant differences in performance when comparing the SVR and GPR models. Thus, we recommend the SVR model as an

TABLE III. MEAN (SD) DIFFERENCES BETWEEN PREDICTED AND MEASURED STANCE HIP, KNEE AND ANKLE MOMENT PARAMTERS (TOP) AND SWING HIP, KNEE AND ANKLE ANGLE PARAMETERS (BOTTOM).

Stance Prediction	Initial Moment Difference (Nm/kg)			Peak Moment Difference (Nm/kg)			Terminal Moment Difference (Nm/kg)		
	Hip	Knee	Ankle	Hip	Knee	Ankle	Hip	Knee	Ankle
Support Vector Regression (SVR)									
Level Walk	0.07 (0.04)[a]	0.01 (0.02)	0.05 (0.03)[a]	0.13 (0.04)	0.10 (0.08)[a]	0.22 (0.04)	0.14 (0.02)[a]	0.05 (0.02)[a]	0.04 (0.00)[a]
Incline Walk	0.03 (0.03)	0.02 (0.00)[a]	0.02 (0.00)	0.08 (0.05)[a]	0.23 (0.12)	0.48 (0.23)[a]	0.15 (0.11)[a]	0.13 (0.07)	0.12 (0.06)
Decline Walk	0.06 (0.00)	0.00 (0.01)	0.05 (0.01)[a]	0.20 (0.06)[a]	0.32 (0.14)	0.08 (0.04)[a]	0.20 (0.11)[a]	0.10 (0.05)	0.14 (0.04)
Overall	**0.06 (0.02)**	**0.01 (0.01)**	**0.04 (0.01)**	**0.14 (0.05)**	**0.22 (0.11)**	**0.26 (0.10)**	**0.16 (0.08)**	**0.09 (0.05)**	**0.10 (0.03)**
Gaussian Process Regression (GPR)									
Level Walk	0.01 (0.00)	0.03 (0.00)	0.00 (0.01)	0.17 (0.02)	0.14 (0.06)	0.12 (0.03)	0.08 (0.03)	0.00 (0.00)	0.06 (0.00)
Incline Walk	0.05 (0.02)	0.00 (0.00)	0.04 (0.01)	0.21 (0.11)	0.27 (0.10)	0.39 (0.21)	0.13 (0.08)	0.11 (0.06)	0.13 (0.04)
Decline Walk	0.06 (0.02)	0.06 (0.01)	0.01 (0.00)	0.31 (0.07)	0.37 (0.07)	0.12 (0.05)	0.18 (0.12)	0.08 (0.06)	0.15 (0.03)
Overall	**0.04 (0.02)**	**0.03 (0.01)**	**0.02 (0.01)**	**0.23 (0.07)**	**0.26 (0.11)**	**0.21 (0.10)**	**0.13 (0.08)**	**0.06 (0.04)**	**0.12 (0.02)**

Swing Prediction	Initial Angle Difference (deg)			Peak Angle Difference (deg)			Terminal Angle Difference (deg)		
	Hip	Knee	Ankle	Hip	Knee	Ankle	Hip	Knee	Ankle
Support Vector Regression (SVR)									
Level Walk	0.43 (0.04)	1.46 (0.24)[a]	0.14 (0.05)	1.78 (1.22)	0.08 (0.58)	0.90 (0.74)	0.25 (1.19)	0.59 (0.63)[a]	0.39 (0.58)
Incline Walk	0.08 (0.32)	2.04 (0.33)	0.29 (0.13)	3.12 (0.33)	0.84 (0.23)	1.33 (0.04)	1.29 (0.80)[a]	4.44 (1.73)	0.73 (0.41)
Decline Walk	0.90 (0.61)	1.22 (0.04)	0.02 (0.08)	1.74 (1.37)	5.54 (0.43)[a]	0.26 (0.13)[a]	0.40 (0.55)	0.74 (0.81)	0.03 (0.30)
Stair Ascent	0.58 (1.29)	9.84 (1.89)	1.70 (1.28)	6.89 (0.90)[a]	3.42 (1.80)[a]	5.00 (1.43)[a]	0.19 (2.75)	4.21 (3.08)	0.87 (0.77)
Stair Descent	0.86 (2.62)	3.75 (1.80)	2.99 (0.86)	3.34 (1.43)	24.98 (1.28)	8.16 (0.68)	0.47 (1.56)	0.47 (0.11)[a]	0.78 (1.24)
Overall	**0.57 (0.98)**	**3.66 (0.86)**	**1.03 (0.48)**	**3.37 (1.05)**	**6.97 (0.87)**	**3.13 (0.60)**	**0.52 (1.37)**	**2.09 (1.27)**	**0.56 (0.66)**
Gaussian Process Regression (GPR)									
Level Walk	0.05 (0.14)	0.60 (0.04)	0.11 (0.24)	1.97 (0.97)	1.51 (0.42)	0.77 (0.89)	0.14 (0.96)	1.76 (1.08)	0.37 (0.94)
Incline Walk	0.35 (0.30)	2.10 (1.20)	0.01 (0.13)	3.37 (0.03)	2.56 (0.86)	2.43 (0.26)	0.03 (0.96)	4.81 (1.80)	0.19 (0.21)
Decline Walk	0.41 (0.37)	0.56 (0.09)	0.41 (0.06)	1.79 (1.51)	6.57 (0.60)	0.69 (0.21)	0.49 (0.84)	1.75 (0.46)	0.12 (0.59)
Stair Ascent	0.33 (1.58)	10.68 (1.23)	1.31 (1.23)	7.94 (0.80)	8.49 (1.93)	5.84 (1.42)	1.30 (1.12)	3.41 (1.22)	0.56 (0.57)
Stair Descent	0.82 (2.45)	4.13 (1.72)	4.00 (0.24)	4.31 (2.01)	25.64 (0.54)	8.53 (0.69)	0.04 (1.57)	6.34 (0.56)	0.62 (0.14)
Overall	**0.39 (0.97)**	**3.61 (0.86)**	**1.17 (0.38)**	**3.88 (1.06)**	**8.95 (0.87)**	**3.65 (0.69)**	**0.40 (1.09)**	**3.61 (1.02)**	**0.37 (0.49)**

a. Significant difference (p<0.05) from paired t-tests comparing absolute value differences of SVR or GPR prediction of joint parameter and measured joint parameter. Absolute differences were calculated as the absolute value of predicted joint parameters subtracted from measured joint parameters. Overall differences were averaged across all tasks for each joint.

optimal model due to its relatively lower computational cost. The present results are promising for future work integrating sonomyography into control systems of powered multiple degree-of-freedom lower-limb exoskeletons and protheses.

Previous researchers have tested volitional control architectures for either continuous position control [8], [32], [33] or torque control [34], [35] for single degree-of-freedom actuated limbs (e.g., knee or ankle) based on mechanical and/ or electromyography sensors. Additionally, sonomyography was used for prediction of ankle dorsiflexion moment for potential control of an ankle exoskeleton or functional electrical stimulation system [15]. This is the first study, to our knowledge, to evaluate sonomyography as an input for *future* control of multiple signal outputs (joint moment and angle) and for multiple degrees-of-freedom (hip, knee and ankle). These results can guide future work that integrates these control schemes into next-generation hardware systems, e.g., [8], [36].

Volitional control is ideal for providing the user full autonomy over the robotic assistive device, and we expect could be essential for non-cyclic activities. To date, many volitional control systems employed in research settings rely on activity mode detection [37]–[40]. The introduction of task independence within the control system increases flexibility and could allow for control of the limb during unknown or unstructured lower-extremity tasks. Semi-volitional control can offer many of the same benefits (e.g., increased maneuverability, task-independent control, etc.), while also reducing the amount of data storage required, and utilizing established control methods, such as torque control and minimum jerk control [8], [35], [36]. For example, given the initial, peak and terminal values for either joint moment during stance or joint angle during swing, the continuous trajectory can be produced by minimum jerk optimization.

There are some limitations of the present work. Online evaluation is required to confirm performance of the predictive framework. However, previous research has established a correlation between offline and online performance of intent recognition [40], [41]. Also, these experiments involved able-bodied subjects, and should be extended to include people with mobility limitations and lower-limb loss during additional lower-extremity tasks. Furthermore, more complex models, could prove to be advantageous.

V. CONCLUSION

This work developed and tested a task-independent predictive framework consisting of multiple forward models for volitional and semi-volitional control of hip, knee and ankle joints of assistive devices using sonomyography of the anterior thigh. Both SVR and GPR models resulted in high accuracy of volitional control trajectories and semi-volitional parameters for the hip, knee and ankle joint moments during stance and joint angles during swing. However, the SVR model required less computational time, which is beneficial for real-time implementation. The ability to infer future joint moment and angle trajectories and parameters in a task-independent framework has many benefits: increased flexibility of the control algorithm, as well as additional time for pre-processing and feature extraction, and mapping of control inputs to device actuation. These results are promising to improve the mobility and overall quality of life of user of assistive technologies.

REFERENCES

[1] V. R. Kumar *et al.*, "Assistive Devices For People With Motor Disabilities," 2007.

[2] D. Shi *et al.*, "A Review on Lower Limb Rehabilitation Exoskeleton Robots," *Chinese J Mech Eng*, vol. 32, no. 1, p. 74, 2019.

[3] M. Windrich *et al.*, "Active lower limb prosthetics: a systematic review of design issues and solutions," *Biomed Eng Online*, vol. 15, no. Suppl 3, p. 140, 2016.

[4] A. M. Simon *et al.*, "Strategies to reduce the configuration time for a powered knee and ankle prosthesis across multiple ambulation modes," in *2013 IEEE 13th International Conference on Rehabilitation Robotics (ICORR)*, 2013, pp. 1–6.

[5] M. R. Tucker *et al.*, "Control strategies for active lower extremity prosthetics and orthotics: a review," *J Neuroeng Rehabil*, vol. 12, no. 1, p. 1, 2015.

[6] A. M. Simon *et al.*, "Powered prosthesis control during walking, sitting, standing, and non-weight bearing activities using neural and mechanical inputs," in *2013 6th International IEEE/EMBS Conference on Neural Engineering (NER)*, 2013, pp. 1174–1177.

[7] T. Lenzi *et al.*, "Speed-Adaptation Mechanism: Robotic Prostheses Can Actively Regulate Joint Torque," *IEEE Robot Autom Mag*, vol. 21, no. 4, pp. 94–107, Dec. 2014.

[8] J. Mendez *et al.*, "Powered knee and ankle prosthesis with indirect volitional swing control enables level-ground walking and crossing over obstacles," *Sci Robot*, vol. 5, no. 44, p. eaba6635, Jul. 2020.

[9] J. M. Donelan *et al.*, "Mechanical work for step-to-step transitions is a major determinant of the metabolic cost of human walking.," *J Exp Biol*, vol. 205, no. Pt 23, pp. 3717–3727, Dec. 2002.

[10] B. E. Lawson *et al.*, "A robotic leg prosthesis: Design, control, and implementation," *IEEE Robot Autom Mag*, 2014.

[11] A. M. Simon *et al.*, "Configuring a powered knee and ankle prosthesis for transfemoral amputees within five specific ambulation modes.," *PLoS One*, vol. 9, no. 6, p. e99387, 2014.

[12] A. S. Dhawan *et al.*, "Proprioceptive Sonomyographic Control: A novel method for intuitive and proportional control of multiple degrees-of-freedom for individuals with upper extremity limb loss," *Sci Rep*, vol. 9, no. 1, p. 9499, Dec. 2019.

[13] J. Shi *et al.*, "Feasibility of controlling prosthetic hand using sonomyography signal in real time: Preliminary study," *J Rehabil Res Dev*, 2010.

[14] S. Sikdar *et al.*, "Novel method for predicting dexterous individual finger movements by imaging muscle activity using a wearable ultrasonic system," *IEEE Trans Neural Syst Rehabil Eng*, 2014.

[15] Q. Zhang *et al.*, "Prediction of Ankle Dorsiflexion Moment by Combined Ultrasound Sonography and Electromyography," *IEEE Trans Neural Syst Rehabil Eng*, vol. 28, no. 1, pp. 318–327, Jan. 2020.

[16] Q. Zhang *et al.*, "Evaluation of Non-Invasive Ankle Joint Effort Prediction Methods for Use in Neurorehabilitation Using Electromyography and Ultrasound Imaging," *IEEE Trans Biomed Eng*, vol. 68, no. 3, pp. 1044–1055, Mar. 2021.

[17] K. G. Rabe *et al.*, "Ultrasound Sensing Can Improve Continuous Classification of Discrete Ambulation Modes Compared to Surface Electromyography," *IEEE Trans Biomed Eng*, vol. 68, no. 4, pp. 1379–1388, Apr. 2021.

[18] K. G. Rabe *et al.*, "Use of Sonomyographic Sensing to Estimate Knee Angular Velocity During Varying Modes of Ambulation," in *2020 42nd Annual International Conference of the IEEE Engineering in Medicine & Biology Society (EMBC)*, Jul. 2020, pp. 3799–3802.

[19] K. G. Rabe *et al.*, "Performance of Sonomyographic and Electromyographic Sensing for Continuous Estimation of Joint Torque During Ambulation on Multiple Terrains," *IEEE Trans Neural Syst Rehabil Eng*, vol. 29, pp. 2635–2644, 2021.

[20] C. Cortes and V. Vapnik, "Support-vector networks," *Mach Learn*, vol. 20, no. 3, pp. 273–297, 1995.

[21] A. Ameri *et al.*, "Support Vector Regression for Improved Real-Time, Simultaneous Myoelectric Control," *IEEE Trans Neural Syst Rehabil Eng*, vol. 22, no. 6, pp. 1198–1209, 2014.

[22] D. W. Kim *et al.*, "Use of Support Vector Regression in Stable Trajectory Generation for Walking Humanoid Robots," *ETRI J*, vol. 31, no. 5, pp. 565–575, Oct. 2009.

[23] C. E. Rasmussen, "Gaussian Processes in Machine Learning," in *Advanced Lectures on Machine Learning: ML Summer Schools 2003, Canberra, Australia, February 2 - 14, 2003, Tübingen, Germany, August 4 - 16, 2003, Revised Lectures*, O. Bousquet, U. von Luxburg, and G. Rätsch, Eds. Berlin, Heidelberg: Springer Berlin Heidelberg, 2004, pp. 63–71.

[24] J. M. Wang *et al.*, "Gaussian Process Dynamical Models for Human Motion," *IEEE Trans Pattern Anal Mach Intell*, vol. 30, no. 2, pp. 283–298, Feb. 2008.

[25] B. Van Hooren *et al.*, "Ultrasound imaging to assess skeletal muscle architecture during movements: a systematic review of methods, reliability, and challenges," *J Appl Physiol*, vol. 128, no. 4, pp. 978–999, Mar. 2020.

[26] A. J. Blazevich *et al.*, "Intra- and intermuscular variation in human quadriceps femoris architecture assessed in vivo.," *J Anat*, vol. 209, no. 3, pp. 289–310, Sep. 2006.

[27] A. J. Tweedell *et al.*, "Differences in muscle contraction onset as determined by ultrasound and electromyography.," *Muscle Nerve*, vol. 59, no. 4, pp. 494–500, Apr. 2019.

[28] P. W. Hodges *et al.*, "Measurement of muscle contraction with ultrasound imaging," *Muscle Nerve*, vol. 27, no. 6, pp. 682–692, 2003.

[29] I. Almohimeed and Y. Ono, "Ultrasound measurement of skeletal muscle contractile parameters using flexible and wearable single-element ultrasonic sensor," *Sensors (Switzerland)*, 2020.

[30] S. Kp *et al.*, *Machine learning with SVM and other kernel methods*. 2009.

[31] N. Zhang *et al.*, "Gaussian Process Regression Method for Classification for High-Dimensional Data with Limited Samples," in *2018 Eighth International Conference on Information Science and Technology (ICIST)*, 2018, pp. 358–363.

[32] T. A. Swift, *Control and Trajectory Generation of a Wearable Mobility Exoskeleton for Spinal Cord Injury Patients*. 2011.

[33] K. H. Ha *et al.*, "Volitional Control of a Prosthetic Knee Using Surface Electromyography," *IEEE Trans Biomed Eng*, vol. 58, no. 1, pp. 144–151, Jan. 2011.

[34] C. D. Hoover *et al.*, "Stair Ascent With a Powered Transfemoral Prosthesis Under Direct Myoelectric Control," *IEEE/ASME Trans Mechatronics*, vol. 18, no. 3, pp. 1191–1200, Jun. 2013.

[35] A. Tsukahara *et al.*, "Restoration of gait for spinal cord injury patients using HAL with intention estimator for preferable swing speed.," *IEEE Trans neural Syst Rehabil Eng a Publ IEEE Eng Med Biol Soc*, vol. 23, no. 2, pp. 308–318, Mar. 2015.

[36] T. Lenzi *et al.*, "Design, development, and testing of a lightweight hybrid robotic knee prosthesis," *Int J Rob Res*, vol. 37, no. 8, pp. 953–976, Jul. 2018.

[37] H. Huang *et al.*, "Design of a robust EMG sensing interface for pattern classification," *J Neural Eng*, vol. 7, no. 5, p. 056005, Oct. 2010.

[38] M. Gordon *et al.*, "Online Learning for Proactive Obstacle Avoidance with Powered Transfemoral Prostheses," in *2019 International Conference on Robotics and Automation (ICRA)*, 2019, pp. 7920–7925.

[39] A. M. Simon *et al.*, "Delaying Ambulation Mode Transition Decisions Improves Accuracy of a Flexible Control System for Powered Knee-Ankle Prosthesis," *IEEE Trans Neural Syst Rehabil Eng*, vol. 25, no. 8, pp. 1164–1171, Aug. 2017.

[40] L. J. Hargrove *et al.*, "Intuitive Control of a Powered Prosthetic Leg During Ambulation," *JAMA*, vol. 313, no. 22, p. 2244, Jun. 2015.

[41] B. Lv *et al.*, "Relationship Between Offline and Online Metrics in Myoelectric Pattern Recognition Control Based on Target Achievement Control Test," in *2019 41st Annual International Conference of the IEEE Engineering in Medicine and Biology Society (EMBC)*, Jul. 2019, pp. 6595–6598.